

# Computation Rate Maximization for Wireless Powered Mobile-Edge Computing with Binary Computation Offloading

Suzhi Bi and Ying Jun (Angela) Zhang

## Abstract

Finite battery lifetime and low computing capability of size-constrained wireless devices (WDs) have been longstanding performance limitations of many low-power wireless networks, e.g., wireless sensor networks (WSNs) and Internet of Things (IoT). The recent development of radio frequency (RF) based wireless power transfer (WPT) and mobile edge computing (MEC) technologies provide promising solutions to fully remove these limitations so as to achieve sustainable device operation and enhanced computational capability. In this paper, we consider a multi-user MEC network powered by WPT, where each energy-harvesting WD follows a binary computation offloading policy, i.e., data set of a task has to be executed as a whole either locally or remotely at the MEC server via task offloading. In particular, we are interested in maximizing the (weighted) sum computation rate of all the WDs in the network by jointly optimizing the individual computing mode selection (i.e., local computing or offloading) and the system transmission time allocation (on WPT and task offloading). The major difficulty lies in the combinatorial nature of multi-user computing mode selection and its strong coupling with transmission time allocation. To tackle this problem, we first consider a decoupled optimization, where we assume that the mode selection is given and propose a simple bi-section search algorithm to obtain the conditional optimal time allocation. On top of that, a coordinate descent method is devised to optimize the mode selection. The method is simple in implementation but may suffer from high computational complexity in a large-size network. To address this problem, we further propose a joint optimization method based on the ADMM (alternating direction method of multipliers) decomposition technique, which enjoys much slower increase of computational complexity as the networks size increases. Extensive simulations show that both the proposed methods can efficiently achieve near-optimal performance under various network setups, and significantly outperform the other representative benchmark methods considered.

## Index Terms

Mobile edge computing, wireless power transfer, binary computation offloading, resource allocation.

S. Bi (bsz@szu.edu.cn) is with the College of Information Engineering, Shenzhen University, Shenzhen, China. Y. J. Zhang (yjzhang@ie.cuhk.edu.hk) is with the Department of Information Engineering, The Chinese University of Hong Kong, HK.

## I. INTRODUCTION

The recent development of Internet of Things (IoT) technology is a key step towards truly intelligent and autonomous control in many important industrial and commercial systems, such as smart power grid and smart home automation [1]. In an IoT network, massive number of wireless devices (WDs) capable of communication and computation are deployed. Due to the stringent device size constraint and production cost consideration, an IoT device (e.g., sensor) often carries a capacity-limited battery and an energy-saving low-performance processor. As a result, the *finite device lifetime* and *low computing capability* are unable to support increasingly many new applications that require sustainable and high-performance computations, e.g., autonomous driving and augmented reality. Therefore, how to tackle the two fundamental performance limitations is a critical problem in the research and development of modern IoT technology.

Recently, radio frequency (RF) based *wireless power transfer* (WPT) has emerged as an effective solution to the finite battery capacity problem [2]–[4]. Specifically, WPT uses dedicated RF energy transmitter, which can continuously charge the battery of remote energy-harvesting devices. Currently, commercial WPT transmitter can effectively deliver tens of microwatts RF power to a distance of more than 10 meters, which is sufficient to power the activities of many low-power WDs [5]. Meanwhile, we expect much more efficient WPT in the near future, considering the fast development of WPT circuit design and advanced signal processing techniques, e.g., energy beamforming [6], [7] and distributed multi-point WPT [8]. The application of WPT to power wireless communication devices has attracted extensive research interests [5], [9], [10]. Thanks to the broadcasting nature of RF signal, WPT is particularly suitable for powering a large number of closely-located WDs, like those deployed in WSNs and IoT.

On the other hand, a recent technology innovation named *mobile edge computing* (MEC) is proposed as a cost-effective method to enhance the computing capability of wireless devices [11], [12]. As its name suggests, MEC allows the WDs to offload intensive computations to nearby servers located at the edge of radio access network, e.g., cellular base station and WiFi access point (AP). Compared with the conventional cloud computing paradigm, MEC removes long backhaul latency, and enjoys lower device energy consumption and superior server load balancing performance. In particular, MEC hits a perfect match with the IoT technology, and thus has attracted massive investment from many major technology companies, such as Huawei, Intel and IBM, and has been identified as a key technology towards future 5G network [13]. In

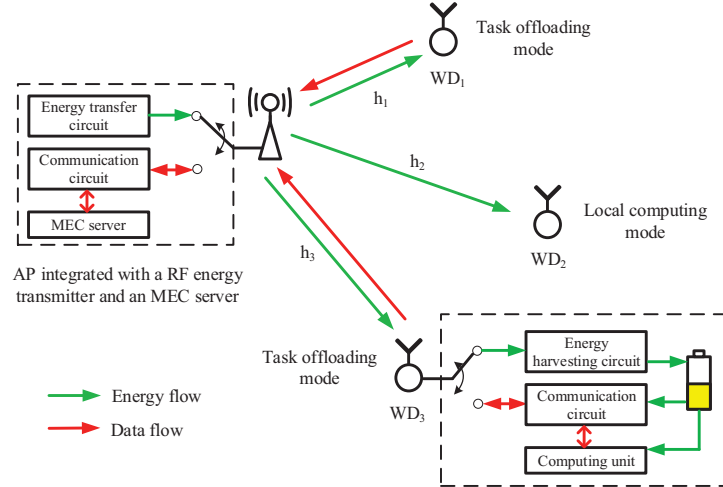


Fig. 1: An example 3-user wireless powered MEC system with binary computation offloading.

general, there are two basic computation task offloading models in MEC, i.e., binary and partial computation offloading [12]. Specifically, *binary offloading* requires a task to be executed as a whole either locally at the WD or remotely at the MEC server. Partial offloading, on the other hand, allows a task to be partitioned into two parts with one executed locally and the other offloaded for edge execution. In practice, binary offloading is easier to implement and suitable for simple tasks that are not partitionable, while partial offloading is favorable for some complex tasks composed of multiple parallel segments.

In conventional battery-powered MEC networks, a key research problem is the joint design of task offloading and system resource allocation to optimize the computing performance [14]–[17]. For a single-user MEC, [14] studies the optimal binary offloading decision to minimize the energy consumption under stochastic wireless channel, where it optimizes the CPU frequency in local computing mode and the transmission data rate in offloading mode. For partial offloading mode, [15] jointly optimizes the offloading ratio, transmission power and CPU frequency to either minimize energy consumption or computation latency. For multi-user MEC with partial offloading, [16] allows the users to share the MEC server in time and formulates a convex optimization to minimize the weighted sum energy consumption of the users by jointly optimizing the offloading ratio and time. Multi-user MEC with binary offloading is a more complicated scenario, which often involves non-convex combinatorial optimization problems. In [17], a heuristic algorithm based on separable semidefinite relaxation is proposed to optimize binary offloading decisions and wireless resource allocation for minimum energy consumptions.

The integration of WPT and MEC technologies introduces a new paradigm named *wireless powered MEC*, which can potentially tackle the two fundamental performance limitations in IoT networks. Meanwhile, it brings new challenges to the optimal system design. On one hand, the task offloading and resource allocation decisions in MEC now depend on the distinct amount of energy harvested by individual WDs from WPT. On the other hand, WPT and task offloading need to share the limited wireless resource, e.g., time or frequency. There are few existing studies on wireless powered MEC system [18]–[20]. [18] considers a single-user wireless powered MEC with binary offloading, where the user maximizes its probability of successful computation under latency constraint. In a multi-user scenario, [19] considers using a multi-antenna AP to power the users and minimizes the AP’s total energy consumption subject to the users’ individual latency constraints. A closely related work to this paper is [20], which maximizes the weighted sum computation rate of a multi-user wireless powered MEC network. However, both [19] and [20] assume partial computation offloading policy. In contrast, the optimal design of binary offloading policy, which is widely adopted in IoT networks by simple computing tasks, is currently lacking of study. Mathematically speaking, partial offloading is a convex-relaxed version of the binary offloading policy, which avoids the hard combinatorial mode selection problem in system design. In fact, both [19] and [20] derived convex optimization formulations, such that the optimal solution can be efficiently obtained with off-the-shelf algorithms. The optimal design under the binary offloading policy in a multi-user environment, however, is a much more challenging problem, which even has not been fully addressed in conventional battery-powered MEC.

In this paper, we consider a wireless powered MEC network as shown in Fig. 1, where the AP is reused as both energy transmitter and MEC server that transfers RF power to and receives computation offload from the WDs. Each device follows the *binary offloading policy*. In particular, we are interested in maximizing the *weighted sum computation rate*, i.e., the number of processed bits per second, of all the WDs in the network, which is a direct measure of the overall computing capability of the system [20]. To the authors’ best knowledge, this is the first paper that studies the optimal design in a multi-user wireless powered MEC network using binary computation offloading policy. Our contributions are detailed below.

- 1) We formulate the problem as a joint optimization of individual computing mode selection (i.e., offloading or local computing) and the system transmission time allocation (on WPT and task offloading). The combinatorial nature of multi-user computing mode selection and its strong coupling with time allocation make the optimal solution hard obtain in general.

As a performance benchmark, a mode enumeration-based optimal method is presented for evaluating the other reduced-complexity algorithms proposed in this paper.

- 2) We first propose a decoupled optimization method. With a given mode selection decision, we derive a semi-closed-form solution of the optimal time allocation. Then, we propose a simple bi-section search algorithm that can efficiently obtain the optimal time allocation. On top of that, a coordinate descent method is devised to optimize the mode selection. The method is simple in implementation as it involves only basic function evaluations. However, the overall computational complexity grows like  $O(N^3)$ , where  $N$  is the network size. As such, the computational complexity may become undesirable when  $N$  is too large.
- 3) To address the complexity issue in large-size networks, we further devise an ADMM-based technique that jointly optimizes the mode selection and time allocation. The proposed method tackles the hard combinatorial mode selection by decomposing the original problem into parallel small-scale integer programming subproblems, one for each WD. Compared to the coordinate descent method, the ADMM-based method requires more complex calculations, e.g., projected Newton's method [21]. On the other hand, its computational complexity increases much more slowly at a linear rate  $O(N)$  of the network size.
- 4) Interestingly, in a special case where all the WDs are homogeneous in terms of computation energy efficiency and weight, we show that the optimal computing mode selection has a *threshold structure* based on the wireless channel strength. Therefore, a simple linear searching method suffices to achieve the globally optimal solution.

Extensive simulations show that both the proposed algorithms can achieve *near-optimal* performance under various network setups, and significantly outperform the other benchmark algorithms. In practice, based on their respective features, it is more preferable to apply the coordinate descent method when network size is small (e.g.,  $\leq 30$  WDs) or the AP is hardware-constrained, and to use ADMM-based method in a large-size network where the impact of network size dominates the overall computational complexity.

The rest of the paper is organized as follows. In Section II, we introduce the system model of the wireless powered MEC. The computation rate maximization problem is formulated in Section III. In Section IV and V, we propose two efficient algorithms to solve the problem with different practical features. In Section VI, simulation results are presented to evaluate the proposed algorithms. Finally, we conclude the paper and discuss future directions in Section VII.

## II. SYSTEM MODEL

### A. Network Model

As shown in Fig. 1, we consider a wireless powered MEC network consisting of an AP and  $N$  WDs, where the AP and the WDs have a single antenna each. In particular, an RF energy transmitter and a MEC server is integrated at the AP. The AP is assumed to be connected to a stable power supply and broadcast RF energy to the distributed WDs, while each WD has an energy harvesting circuit and a rechargeable battery that can store the harvested energy to power its operations. Each device, including the AP and the WDs, has a communication circuit. Specifically, we assume that WPT and communication are performed in the same frequency band. To avoid mutual interference, the communication and energy harvesting circuits of each WD operate in a time-division-multiplexing (TDD) manner. A similar TDD circuit structure is also applied at the AP to separate energy transmission and communication with the WDs. Within each system time frame of duration  $T$ , the wireless channel gain between the AP and the  $i$ -th WD is denoted by  $h_i$ , which is assumed reciprocal for the downlink and uplink,<sup>1</sup> and static within each time frame but may vary across different time frames.

Within each time frame, we assume that each WD needs to accomplish a certain computing task based on its local data. For instance, a WD as a wireless sensor needs to regularly generate an estimate, e.g., the pollution level of the monitored area, based on the raw data samples measured from the environment. In particular, the computing task of a WD can be performed locally by the on-chip micro-processor, which has low computing capability due to the energy- and size-constrained computing processor. Alternatively, the WD can also offload the data to the MEC server with much more powerful processing power, which will compute the task and send the result back to the WD.

In this paper, we assume that the WDs adopt a binary computation offloading rule. That is, a WD must choose to operate in either the local computing mode (mode 0, like WD<sub>2</sub> in Fig. 1) or the offloading mode (mode 1, like WD<sub>1</sub> and WD<sub>3</sub>) in each time frame. In practice, this corresponds to a wide variety of applications. For instance, the measurement samples of a sensor are correlated in time, and thus need to be jointly processed to enhance the estimation accuracy.

<sup>1</sup>The channel reciprocity assumption is made to obtain more design insights on the impact of wireless channel conditions. The proposed algorithms in this paper, however, can be easily extended to the case with non-equal uplink and downlink channels.

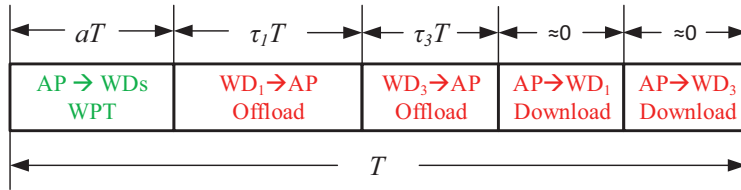


Fig. 2: An example time allocation in the 3-user wireless powered MEC network in Fig. 1. Only WD<sub>1</sub> and WD<sub>3</sub> selecting mode 1 offload the task to and download the computation results from the AP.

### B. Computation Model

We consider an example transmission time allocation in Fig. 2. We use two non-overlapping sets  $\mathcal{M}_0$  and  $\mathcal{M}_1$  to denote the indices of WDs that operate in mode 0 and 1, respectively. As such  $\mathcal{M} = \mathcal{M}_0 \cup \mathcal{M}_1 = \{1, \dots, N\}$  is the set of all the WDs. In the first part of a tagged time frame, the AP broadcasts wireless energy to the WDs for  $aT$  amount of time, where  $a \in [0, 1]$ , and all the WDs harvest the energy. Specifically, the energy harvested by the  $i$ -th WD is

$$E_i = \mu P h_i a T, \quad i = 1, \dots, N, \quad (1)$$

where  $P$  denotes the RF energy transmit power of the AP and  $\mu \in (0, 1)$  denotes the energy harvesting efficiency [6]. In the second part of the time frame  $(1 - a)T$ , the WDs in  $\mathcal{M}_1$  (e.g., WD<sub>1</sub> and WD<sub>3</sub> in Fig. 1) offload the data to the AP. To avoid co-channel interference, we assume that the WDs take turns to transmit in the uplink, and the time that a WD <sub>$i$</sub>  transmits is denoted by  $\tau_i T$ ,  $\tau_i \in [0, 1]$ . Depending on the selected computing mode, the detailed operation of each WD is illustrated as follows.

1) *Local Computing Mode*: Notice that the energy harvesting circuit and the computing unit are separate. Thus, a mode-0 WD can *harvest energy and compute its task simultaneously*. That is, it can compute throughout the entire time frame of duration  $T$ . Let  $\phi > 0$  denote the number of computation cycles needed to process one bit of raw data, which is determined by the nature of the application and is assumed to be equal for all the WDs. Let  $f_i$  denote the processor's chosen computing speed (cycles per second) and  $0 \leq t_i \leq T$  denote the computation time of the WD.  $f_i \leq f_{max}$  holds as the computation capability constraint. The power consumption of the processor is modeled as  $k_i f_i^3$  (joule per second), where  $k_i$  denotes the computation energy efficiency coefficient of the processor's chip [15]. Then, the total energy consumption is constrained by

$$k_i f_i^3 t_i \leq E_i \quad (2)$$

to ensure sustainable operation of the WD.<sup>2</sup> In particular, we assume that the WDs are *energy-constrained*, such that a WD can always consume all the harvested energy within a time frame by operating at the maximum computing speed. In other words,

$$E_i = \mu P h_i a T \leq \mu P h_i T < k_i f_{max}^3 T \quad (3)$$

holds for any practical value of  $h_i$  and  $i = 1, \dots, N$ . With the above computation model, the computation rate of WD<sub>*i*</sub> (in bits per second) denoted by  $r_i$ , can be calculated as [15]

$$r_i = \frac{f_i t_i}{\phi T}, \quad \forall i \in \mathcal{M}_0. \quad (4)$$

2) *Offloading Mode*: Due to the TDD circuit constraint, a mode-1 WD can only *offload its task to the AP after harvesting energy*. We denote the number of bits to be offloaded to the AP as  $v_u b_i$ , where  $b_i$  denotes the amount of raw data and  $v_u > 1$  indicates the communication overhead in task offloading, such as packet header and encryption. Let  $P_i$  and  $\tau_i$  denote the transmit power and time of the  $i$ -th WD, respectively. Then, we have

$$b_i \leq \frac{B \tau_i T}{v_u} \log_2 \left( 1 + \frac{P_i h_i}{N_0} \right), \quad \forall i \in \mathcal{M}_1, \quad (5)$$

where  $B$  denotes the communication bandwidth and  $N_0$  denotes the receiver noise power.

After receiving the raw data of all the WDs, the AP computes and sends back the output result of length  $r_d b_i$  bits back to the corresponding WD. Here,  $r_d \ll 1$  indicates the output/input ratio including the overhead in downlink transmission. Let  $f_0$  denote the AP processor's fixed computing speed and  $P_0$  denote the transmit power of the AP. The time spent on task computation and feeding back to WD<sub>*i*</sub> is

$$v_i = \frac{\phi b_i}{f_0} + \frac{r_d b_i}{B \log_2 \left( 1 + \frac{P_0 h_i}{N_0} \right)}. \quad (6)$$

In practice, the computing capability and the transmit power of the AP is much stronger than the energy-harvesting WDs, e.g., by more than three orders of magnitude. Beside,  $r_d$  is a very small value, e.g., one output temperature estimation from tens of input sensing sample. Accordingly, we can infer from (5) and (6) that  $v_i \ll \tau_i$ , and thus the time spent on task computation and

<sup>2</sup>We assume each WD has sufficient initial energy in the very beginning and the battery capacity is sufficiently large such that battery-overcharging is negligible.

result feedback by the AP can be safely neglected like in [14], [18], [19]. In this case, task offloading can occupy the rest of the time frame after WPT, i.e.,

$$\sum_{i \in \mathcal{M}_1} \tau_i + a \leq 1. \quad (7)$$

Besides, from the above discussion, we also neglect the energy consumption by the WD on receiving the computation result from the AP, and consider only the energy consumptions on data transmission to the AP. In this case, we have  $P_i \tau_i \leq E_i$ . Then, the computation rate of a mode-1 WD<sub>*i*</sub> is upper bounded as

$$r_i = \frac{b_i}{T} \leq \frac{B\tau_i}{v_u} \log_2 \left( 1 + \frac{\mu P a h_i^2}{\tau_i N_0} \right), \quad \forall i \in \mathcal{M}_1. \quad (8)$$

Due to the stringent energy and computation limitations of the WDs, we adopt a centralized control scheme where the AP is responsible for all the computations and coordinations, including selecting the computing mode for each WD. In the next section, we formulate the weighted sum-rate maximization problem of the considered wireless powered MEC system.

### III. PROBLEM FORMULATION

In this paper, we maximize the weighted sum computation rate of all the WDs in each time frame. In this case, the equality in (8) holds by letting  $P_i = \frac{E_i}{\tau_i}$ .<sup>3</sup> From (4) and (8), we can see that the computation rates of the WDs are related to their computing mode selection and the system resource allocation on WPT, communication, and computation. Mathematically, the computation rate maximization problem is formulated as follows.

$$(P1) : \quad \underset{\mathcal{M}_0, a, \tau, \mathbf{f}, \mathbf{t}}{\text{maximize}} \quad \sum_{i \in \mathcal{M}_0} w_i \frac{f_i t_i}{\phi T} + \sum_{j \in \mathcal{M}_1} w_j \frac{B\tau_j}{v_u} \log_2 \left( 1 + \frac{\mu P a h_j^2}{\tau_j N_0} \right) \quad (9a)$$

$$\text{subject to} \quad \sum_{j \in \mathcal{M}_1} \tau_j + a \leq 1, \quad (9b)$$

$$k_i f_i^3 t_i \leq \mu P h_i a T, \quad \forall i \in \mathcal{M}_0, \quad (9c)$$

$$0 \leq t_i \leq T, \quad 0 \leq f_i \leq f_{max}, \quad \forall i \in \mathcal{M}_0, \quad (9d)$$

$$a \geq 0, \quad \tau_j \geq 0, \quad \forall j \in \mathcal{M}_1, \quad (9e)$$

$$\mathcal{M}_0 \subseteq \mathcal{M}, \quad \mathcal{M}_1 = \mathcal{M} \setminus \mathcal{M}_0. \quad (9f)$$

<sup>3</sup>Same as most of the existing work on wireless powered communications, e.g., [9], [10], we do not assume a maximum transmit power constraint for the WDs because of the small amount energy harvested from WPT in practice.

Here,  $w_i > 0$  denotes the weight of the  $i$ -th WD.  $\mathbf{f} = \{f_i | i \in \mathcal{M}_0\}$  and  $\mathbf{t} = \{t_i | i \in \mathcal{M}_0\}$  denote the computing speed and computation time of the mode-0 WDs.  $\boldsymbol{\tau} = \{\tau_j | j \in \mathcal{M}_1\}$  denotes the offloading time of the mode-1 WDs. The two terms of the objective function correspond to the computation rates of mode-0 and mode-1 WDs, respectively. (9b) is the time allocation constraint and (9c) denotes the individual energy harvesting constraints for mode-0 WDs.

Problem (P1) is evidently non-convex due to the combinatorial mode selection variable  $\mathcal{M}_0$  and the multiplicative terms in both the objective function and constraints. A close observation of (P1) shows that we can independently optimize the computing speed  $f_i$  and duration  $t_i$  of each mode-0 WD $_i$  without affecting the performance of the other WDs, when the WPT time  $aT$  is fixed. Specifically, for a tagged mode-0 WD $_i$ , we have

$$r_i = \frac{f_i t_i}{\phi T} \leq \frac{1}{\phi_i T} \left( \frac{E_i}{k_i} \right)^{\frac{1}{3}} t_i^{\frac{2}{3}}, \quad (10)$$

where the inequality is obtained from (2). Note that  $r_i$  increases with  $t_i$  in (10). Hence, the maximum  $r_i^*$  is achieved by setting  $t_i^* = T$ , i.e., the WD computes for a maximal allowable time throughout the time frame and at a minimal possible computing speed. Accordingly, we have  $f_i^* = \min \left( \left( \frac{E_i}{k_i T} \right)^{\frac{1}{3}}, f_{max} \right)$ . By the assumption in (3), we can infer that  $\left( \frac{E_i}{k_i T} \right)^{\frac{1}{3}} < f_{max}$  always holds. Thus,  $f_i^* = \left( \frac{E_i}{k_i T} \right)^{\frac{1}{3}}$ . By substituting  $t_i^* = T$  and  $f_i^* = \left( \frac{E_i}{k_i T} \right)^{\frac{1}{3}}$  into (4), the maximum computation rate is

$$r_i^* = \frac{f_i^* t_i^*}{\phi T} = \eta_1 \left( \frac{h_i}{k_i} \right)^{\frac{1}{3}} a^{\frac{1}{3}}, \quad \forall i \in \mathcal{M}_0, \quad (11)$$

where  $\eta_1 \triangleq \frac{(\mu P)^{\frac{1}{3}}}{\phi}$  is a fixed parameter.

From the above analysis, we can replace the first term in (P1) with the RHS of (11) to safely remove the variables  $\mathbf{f}$ ,  $\mathbf{t}$  and the corresponding constraints in (9c) and (9d). This yields an equivalent simplification of (P1):

$$(P2) : \underset{\mathcal{M}_0, a, \boldsymbol{\tau}}{\text{maximize}} \quad \sum_{i \in \mathcal{M}_0} w_i \eta_1 \left( \frac{h_i}{k_i} \right)^{\frac{1}{3}} a^{\frac{1}{3}} + \sum_{j \in \mathcal{M}_1} w_j \varepsilon \tau_j \ln \left( 1 + \frac{\eta_2 h_j^2 a}{\tau_j} \right) \quad (12a)$$

$$\text{subject to} \quad \sum_{j \in \mathcal{M}_1} \tau_j + a \leq 1, \quad (12b)$$

$$a \geq 0, \tau_j \geq 0, \forall j \in \mathcal{M}_1, \mathcal{M}_0 \subseteq \mathcal{M}, \mathcal{M}_1 = \mathcal{M} \setminus \mathcal{M}_0, \quad (12c)$$

where  $\eta_2 \triangleq \frac{\mu P}{N_0}$  and  $\varepsilon \triangleq \frac{B}{v_u \ln 2}$ . Among all the parameters in (P2), the AP only needs to estimate the wireless channel gains  $h_i$ 's that are time varying in each time frame. The others are static

parameters that remain constant for sufficiently long period of time, such as  $w_i$ 's and  $k_i$ 's. Then, the AP calculates (P2) and broadcasts the solution  $\{\mathcal{M}_0^*, a^*, \tau^*\}$  to the WDs, which will react by operating in their designated computing modes.<sup>4</sup>

(P2) is still a hard non-convex problem due to the combinatorial computing mode selection. However, we observe that the second term in the objective is jointly concave in  $(a, \tau_j)$ . Once  $\mathcal{M}_0$  is given, (P2) reduces to a convex problem, where the optimal time allocation  $\{a^*, \tau^*\}$  can be efficiently solved using off-the-shelf optimization algorithms, e.g., interior point method [21]. Accordingly, a straightforward method is to enumerate all the  $2^N$  possible  $\mathcal{M}_0$  and output the one that yields the highest objective value. The pattern enumeration method may be applicable for a small number of WDs, e.g.,  $N \leq 10$ . It quickly becomes computationally infeasible as  $N$  further increases, especially for delay-sensitive applications. Therefore, it will be mainly used as a benchmark to evaluate the performance of the proposed reduced-complexity algorithms in this paper. Before entering formal discussions on the algorithm design, it is worth mentioning that a closely related max-min rate optimization problem, which maximizes the minimum computation rate among the WDs, has its dual problem in the form of weight-sum-rate-maximization like (P2). In this sense, the proposed methods in this paper can also be extended to enhance the *user fairness* in a wireless powered MEC system.

#### IV. DECOUPLED OPTIMIZATION USING COORDINATE DESCENT METHOD

In this section, we propose a decoupled optimization method, where we first assume that  $\mathcal{M}_0$  is given and derive a semi-closed-form expression of the optimal time allocation  $\{a^*, \tau^*\}$ . Subsequently, a low-complexity bi-section search can be applied to obtain the optimal solution. On top of that, we further devise a coordinate descent method that optimizes the mode selection. Interestingly, we prove that the optimal computing mode selection of a special case, where the WDs are homogeneous in terms of weight and computing efficiency, has a threshold structure. Based on it, the global optimal solution can be efficiently obtained via simple linear search.

##### A. Optimal Transmission Time Allocation Given $\mathcal{M}_0$

In this subsection, we study the optimal transmission time allocation problem in (P2) given  $\mathcal{M}_0$ . In particular, we propose a simple bi-section search algorithm that has much lower complexity

<sup>4</sup>The energy and time consumed on channel estimation and coordination can be modeled as two constant terms that will not affect the validity of the proposed algorithms. For simplicity of illustration, they are neglected in this paper.

than general convex optimization techniques, e.g., interior point method. Besides, interesting design insights are obtained from the analysis in this subsection.

Suppose that  $\mathcal{M}_0$  is given in (P2). Let us introduce a Lagrangian multiplier to constraint (12b) to form a partial Lagrangian

$$L(a, \boldsymbol{\tau}, \nu) = \sum_{i \in \mathcal{M}_0} w_i \eta_1 \left( \frac{h_i}{k_i} \right)^{\frac{1}{3}} a^{\frac{1}{3}} + \sum_{j \in \mathcal{M}_1} w_j \varepsilon \tau_j \ln \left( 1 + \frac{\eta_2 h_j^2 a}{\tau_j} \right) + \nu \left( 1 - a - \sum_{j \in \mathcal{M}_1} \tau_j \right). \quad (13)$$

The corresponding dual function is

$$d(\nu) = \underset{a, \boldsymbol{\tau}}{\text{maximize}} \{L(a, \boldsymbol{\tau}, \nu) \mid a \geq 0, \tau_j \geq 0, \forall j \in \mathcal{M}_1\}, \quad (14)$$

and the dual problem is

$$\underset{\nu}{\text{minimize}} \{d(\nu) \mid \nu \geq 0\}. \quad (15)$$

As (P2) is a convex problem given  $\mathcal{M}_0$ , the dual problem achieves the same optimal objective value by the strong duality. It can be seen that equation  $\sum_{j \in \mathcal{M}_1} \tau_j^* + a^* = 1$  holds at the optimal solution. The following Lemma establishes the relation among  $\{a^*, \boldsymbol{\tau}^*, \nu^*\}$ .

**Lemma 1:** The optimal  $\{a^*, \boldsymbol{\tau}^*, \nu^*\}$  satisfies

$$\frac{\tau_j^*}{a^*} = \frac{\eta_2 h_j^2}{-\left(W\left(-\frac{1}{\exp(1 + \frac{\nu^*}{w_j \varepsilon})}\right)\right)^{-1} - 1}, \quad \forall j \in \mathcal{M}_1, \quad (16)$$

where  $W(x)$  denotes the Lambert-W function, which is the inverse function of  $f(z) = z \exp(z) = x$ , i.e.,  $z = W(x)$ .

*Proof:* Please see the detailed proof in the Appendix A. ■

We can infer from (16) that  $\nu^* > 0$  holds strictly, because otherwise either  $\tau_j^* \rightarrow \infty$  or  $a^* \rightarrow 0$  must hold, which are evidently not true at optimum. When  $\nu^* > 0$ , we have  $-1/e < -\frac{1}{\exp(1 + \frac{\nu^*}{w_j \varepsilon})} < 0$ . As  $W(x) \in (-1, 0)$  when  $x \in (-1/e, 0)$ , the denominator of the RHS of (16) is always positive. Meanwhile, because  $W(x)$  is an increasing function when  $x \in (-1/e, 0)$ , we can infer that a longer offloading time  $\tau_j^*$  is allocated to WD with stronger wireless channels (larger  $h_j$ ) and larger weight  $w_j$ . Let us denote (16) as

$$\tau_j^* = \eta_2 h_j^2 a^* \cdot \varphi_j(\nu^*), \quad \forall j \in \mathcal{M}_1, \quad (17)$$

where

$$\varphi_j(\nu) \triangleq \left[ -\left(W\left(-\frac{1}{\exp(1 + \frac{\nu}{w_j \varepsilon})}\right)\right)^{-1} - 1 \right]^{-1} \quad (18)$$

is a decreasing function in  $\nu$ , with  $\varphi_j(\nu) \rightarrow \infty$  when  $\nu \rightarrow 0$ , and  $\varphi_j(\nu) \rightarrow 0$  when  $\nu \rightarrow \infty$ .

By substituting (17) into  $\sum_{j \in \mathcal{M}_1} \tau_j^* + a^* = 1$ , we obtain a semi-closed-form of  $a^*$  as a function of  $\nu^*$

$$a^* = \frac{1}{1 + \eta_2 \left( \sum_{j \in \mathcal{M}_1} h_j^2 \varphi_j(\nu^*) \right)} \triangleq p_1(\nu^*). \quad (19)$$

Given the monotonicity of  $\varphi_j(\nu^*)$ , we can infer that  $p_1(\nu)$  is an increasing function in  $\nu$ . In particular,  $p_1(\nu) \rightarrow 0$  when  $\nu \rightarrow 0$ , and  $p_1(\nu) \rightarrow 1$  when  $\nu \rightarrow \infty$ .

Now, let us take the partial derivative of  $L$  in (13) with respect to  $a$ . The maximum of  $L$  is achieved when

$$\frac{\partial L}{\partial a} = \frac{1}{3}(a^*)^{-\frac{2}{3}} \sum_{i \in \mathcal{M}_0} w_i \eta_1 \left( \frac{h_i}{k_i} \right)^{\frac{1}{3}} + \sum_{j \in \mathcal{M}_1} \frac{w_j \varepsilon \eta_2 h_j^2}{1 + \eta_2 h_j^2 a^* (\tau_i^*)^{-1}} - \nu = 0. \quad (20)$$

From (17), it holds that

$$\eta_2 h_j^2 a^* (\tau_i^*)^{-1} = \frac{1}{\varphi_j(\nu^*)}. \quad (21)$$

By substituting (19) and (21) into (20), we see that the optimal  $\nu^*$  must satisfy

$$Q(\nu^*) \triangleq \frac{1}{3} (p_1(\nu^*))^{-\frac{2}{3}} \sum_{i \in \mathcal{M}_0} w_i \eta_1 \left( \frac{h_i}{k_i} \right)^{\frac{1}{3}} + \varepsilon \eta_2 \sum_{j \in \mathcal{M}_1} \frac{w_j h_j^2}{1 + 1/\varphi_j(\nu^*)} - \nu^* = 0. \quad (22)$$

Correspondingly, the optimal  $\nu^*$  can be efficiently obtained based on the following proposition.

**Proposition 1:**  $Q(\nu)$  is a monotonically decreasing function in  $\nu > 0$ . Besides, a unique  $\nu^* > 0$  that satisfies  $Q(\nu^*) = 0$  exists.

*Proof:* Notice that  $p_1(\nu)$  is an increasing function in  $\nu$  and  $\varphi_j(\nu)$  is a decreasing function in  $\nu$ . Therefore, all the three terms in  $Q(\nu)$  decrease with  $\nu$ , thus  $Q(\nu)$  is a monotonically decreasing function in  $\nu$ . Meanwhile, when  $\nu \rightarrow 0$ , it holds that  $p_1(\nu) \rightarrow 0$  and  $\varphi_j(\nu) \rightarrow \infty$ . Thus, we have  $Q(\nu) \rightarrow \infty$  when  $\nu \rightarrow 0$ . Besides, when  $\nu \rightarrow \infty$ , it holds that  $p_1(\nu) \rightarrow 1$  and  $\varphi_j(\nu) \rightarrow 0$ , which leads to  $Q(\nu) \rightarrow -\infty$  when  $\nu \rightarrow \infty$ . Together with the result that  $Q(\nu)$  is a monotonically decreasing function, there must exist a unique  $\nu > 0$  that satisfies  $Q(\nu) = 0$ . ■

Now that (P2) is convex given  $\mathcal{M}_0$ ,  $Q(\nu^*) = 0$  is a sufficient condition for optimality. With Proposition 1, the optimal  $\nu^*$  can be efficiently obtained via a bi-section search over  $\nu \in (0, \bar{\nu})$  to find the unique  $\nu$  that satisfies  $Q(\nu) = 0$ , where  $\bar{\nu}$  is a sufficiently large value. Now that the optimal  $\nu^*$  is obtained, the optimal  $\{a^*, \boldsymbol{\tau}^*\}$  can be directly calculated using (17) and (19). Due to the convexity, the primal and dual optimal values are the same for (P2) given  $\mathcal{M}_0$ . The pseudo-code of the bi-section search method is illustrated in Algorithm 1. Given a precision parameter  $\sigma_0$ , it takes  $O\left(\log_2\left(\frac{\bar{\nu}}{\sigma_0}\right)\right)$  number iterations for Algorithm 1 to converge.

In each iteration, the computational complexity of evaluating  $Q(\nu)$  is proportional to the number of WDs, i.e.,  $O(N)$ . Therefore, the overall complexity of Algorithm 1 is  $O(N)$ . Compared with conventional interior point method with  $O(N^3)$  complexity [21], the proposed algorithm significantly reduces the computational cost especially for large  $N$ . Besides, the calculation of the proposed algorithm involves only basic function evaluations, which is much easier to implement in hardware-constrained IoT networks than generic convex optimization algorithms.

---

**Algorithm 1:** Bi-section search algorithm for optimal transmission time allocation

---

**input** : WD mode selection  $\{\mathcal{M}_0, \mathcal{M}_1\}$   
**output** : the optimal  $\{a^*, \tau^*\}$  to Problem (P2) given  $\mathcal{M}_0$

- 1 **initialization**:  $\sigma_0 \leftarrow 0.005$ ,  $\bar{\nu} \leftarrow$  sufficiently large value;
- 2  $UB \leftarrow \bar{\nu}$ ,  $LB \leftarrow 0$ ;
- 3 **repeat**
- 4      $\nu \leftarrow \frac{UB+LB}{2}$ ;
- 5     **if**  $Q(\nu) > 0$  in the LHS of (22) **then**
- 6          $LB \leftarrow \nu$ ;
- 7     **else**
- 8          $UB \leftarrow \nu$ ;
- 9     **end**
- 10 **until**  $|UB - LB| \leq \sigma_0$ ;
- 11 Calculate  $a^*$  using (19), and  $\tau^*$  using  $a^*$  and (17);
- 12 **Return**  $\{a^*, \tau^*\}$ ;

---

### B. Coordinate Descent Method for Computing Mode Optimization

We now proceed to propose a simple coordinate descent method to optimize  $\mathcal{M}_0$ . Specifically, we start with an initial  $\mathcal{M}_0^0$  (thus  $\mathcal{M}_1^0$ ). Let  $\mathcal{M}_0^{l-1}$  denote the mode selection decision at the  $(l-1)$ -th iteration. Correspondingly, we denote  $V(\mathcal{M}_0^{l-1})$  as the optimal value of (P2) given  $\mathcal{M}_0^{l-1}$ , which can be obtained using Algorithm 1. Let  $r_j^l$  denote the reward if WD $_j$  swaps its current computing mode in the  $l$ -th iteration, defined as the increase of objective value of (P2) after the swapping, i.e.,

$$r_j^l = V(\mathcal{M}_0^{l-1}(j)) - V(\mathcal{M}_0^{l-1}), \quad (23)$$

where  $\mathcal{M}_0^{l-1}(j)$  denotes the mode selection after  $\text{WD}_j$  swaps its current mode, i.e.,

$$\mathcal{M}_0^{l-1}(j) = \begin{cases} \mathcal{M}_0^{l-1} \setminus j, & \text{if } j \in \mathcal{M}_0^{l-1}, \\ \mathcal{M}_0^{l-1} \cup j & \text{if } j \in \mathcal{M}_1^{l-1}. \end{cases} \quad (24)$$

Then, the mode selection in the  $l$ -th iteration,  $\mathcal{M}_0^l$ , is obtained by letting the WD that achieves the largest reward swap its mode selection, if such swapping yields a positive reward. In other words,  $\mathcal{M}_0^l = \mathcal{M}_0^{l-1}(j_i^*)$  if  $r_{j_i^*}^l > 0$ , where  $j_i^* = \arg \max_{j=1, \dots, N} r_j^l$ . The pseudo-code of the method is depicted in Algorithm 2. The objective function value of (P2) increases monotonically as the iterations proceed. Meanwhile, the optimal value of (P2) is bounded. Therefore, the coordinate descent method guarantees to converge. In the next subsection, we will show that in a special case with homogeneous WDs, the optimal  $\mathcal{M}_0^*$  has a threshold structure, and thus can be easily obtained through a simple linear search over the  $N$  WDs.

---

**Algorithm 2:** Coordinate descent algorithm for mode selection optimization.

---

**input** : Initial mode selection  $\mathcal{M}_0^0$   
**output** : An approximate solution  $\{\bar{a}, \bar{\tau}, \bar{\mathcal{M}}_0\}$  to (P2)

- 1 **initialization:**  $l \leftarrow 0$ ;
- 2 **repeat**
- 3      $l \leftarrow l + 1$ ;
- 4     **for** each  $\text{WD}_j$  **do**
- 5         Calculate  $r_j^l$  in (23) using Algorithm 1;
- 6     **end**
- 7      $v_i^* \leftarrow \max_{j=1, \dots, N} r_j^l$  and  $j_i^* \leftarrow \arg \max_{j=1, \dots, N} r_j^l$ ;
- 8     Update  $\mathcal{M}_0^l \leftarrow \mathcal{M}_0^{l-1}(j_i^*)$  using (24);
- 9 **until**  $v_i^* \leq 0$ ;
- 10  $\bar{\mathcal{M}}_0 \leftarrow \mathcal{M}_0^{l-1}$ ,  $\{\bar{a}, \bar{\tau}\} \leftarrow$  the optimal solution of (P2) given  $\bar{\mathcal{M}}_0$ ;
- 11 **Return** An approximate solution  $\{\bar{a}, \bar{\tau}, \bar{\mathcal{M}}_0\}$  to (P2);

---

### C. A Homogeneous Special Case

We consider a special case where the WDs are homogeneous in terms of the weight and computation energy efficiency, i.e.,  $w_i = w$  and  $k_i = k$ ,  $\forall i \in \mathcal{M}$ . In this case, the WDs differ only by the wireless channel gain  $h_i$ 's. The following Proposition 2 shows that the optimal computing mode selection has a threshold structure based on the wireless channel gains.

**Proposition 2:** In a wireless powered MEC system with  $N$  homogeneous WDs, i.e.,  $w_i = w$  and  $k_i = k, \forall i \in \mathcal{M}$ . We assume without loss of generality that  $h_1 \geq h_2 \geq \dots \geq h_N$ . Then, there exists an integer  $n \in \{0, 1, \dots, N\}$ , such that the optimal mode selection to (P2) satisfies  $\mathcal{M}_1^* = \{i \leq n \mid i = 1, \dots, N\}$  and  $\mathcal{M}_0^* = \{i > n \mid i = 1, \dots, N\}$ .

*Proof:* Please see the detailed proof in Appendix B. ■

In two extreme cases with  $n = 0$  or  $N$ , all the WDs select local computing or task offloading, respectively. That is,  $\{\mathcal{M}_0^*, \mathcal{M}_1^*\} = \{\mathcal{M}, \emptyset\}$  when  $n = 0$ , and  $\{\mathcal{M}_0^*, \mathcal{M}_1^*\} = \{\emptyset, \mathcal{M}\}$  when  $n = N$ . In general, Proposition 2 provides a necessary condition for the optimal mode selection of the homogeneous special case. That is, any mode-1 WD has stronger channel than the mode-0 WDs at the optimum. Therefore, we can first rank the WDs in a descending order based on their channel gains  $h_i$ 's. Then, we solve (P2) using Algorithm 1 for  $(N + 1)$  times via a linear search from  $n = 0$  to  $N$ , where each  $n$  corresponds to a mode selection  $\{\mathcal{M}_0, \mathcal{M}_1\}$ , and output the one that yields the highest objective. The computational complexity of the linear search approximately equals to that of one iteration of Algorithm 2 used for solving a general case.

We also observe for the special case that the computation rate of a mode-1 WD with weak channel can be significantly lower than that of another mode-1 WD with strong channel. To see this, for those mode-1 WDs, it holds that  $\varphi_j(\nu^*)$ 's in (18) are equal at optimum given the same  $w_j = w$ . Accordingly, we denote  $\varphi_j(\nu^*) = \varphi(\nu^*), \forall j \in \mathcal{M}_1$ , and express the optimal computation rate of a mode-1 WD $_j$  by substituting (17) to (8), where

$$r_j^* = h_j^2 \cdot \varepsilon \eta_2 a \varphi(\nu^*) \ln \left( 1 + \frac{1}{\varphi(\nu^*)} \right), \quad \forall j \in \mathcal{M}_1. \quad (25)$$

It can be shown that  $r_j^*$  decreases with  $\nu^*$ , where  $\nu^*$  can be considered as the ‘‘price’’ of the offloading time charged to the mode-1 WDs. Besides, we can infer from (25) that the mode-1 WDs offload to the AP at the *same spectral efficiency*, but with different durations that are proportional to the square of wireless channel gain (indeed the product of uplink and downlink channel gains). Overall, the computation rates are proportional to  $h_j^2$ 's as well. Intuitively, this is caused by both channel-related energy harvesting in the downlink and task offloading in the uplink. Then, a mode-1 WD with relatively weak channel (say 1/10 of another mode-1 WD) may have much lower computation rate than the other mode-1 WDs (1/100 in this case).

## V. JOINT OPTIMIZATION USING ADMM-BASED METHOD

The major advantage of the coordinate descent method proposed in the last section is its simplicity in implementation, because the computation involves basic function evaluations only.

However, its convergence rate is susceptible to the choice of initial mode selection and the dimension of searching space (i.e., the network size  $N$ ). To address the problem especially in large-size networks, we propose in this section an ADMM-based algorithm to jointly optimize the computing mode selection and transmission time allocation. As we will show later, the proposed ADMM-based approach has a computational complexity that increases slowly with the network size  $N$ .

The main idea is to decompose the hard combinatorial optimization (P2) into  $N$  parallel smaller integer programming problems, one for each WD. Nonetheless, conventional decomposition techniques, such as dual decomposition, cannot be directly applied to (P2) due to the coupling variable  $a$  and constraint (12b) among the WDs. To eliminate these coupling factors, we first reformulate (P2) as an equivalent integer programming problem by introducing binary decision variables  $m_i$ 's and additional artificial variables  $x_i$ 's and  $z_i$ 's as follows

$$(P3) : \underset{a, \mathbf{z}, \mathbf{x}, \boldsymbol{\tau}, \mathbf{m}}{\text{maximize}} \quad \sum_{i=1}^N w_i \left\{ (1 - m_i) \eta_1 \left( \frac{h_i}{k_i} \right)^{\frac{1}{3}} x_i^{\frac{1}{3}} + m_i \varepsilon \tau_i \ln \left( 1 + \frac{\eta_2 h_i^2 x_i}{\tau_i} \right) \right\} \quad (26a)$$

$$\text{subject to} \quad \sum_{i=1}^N z_i + a \leq 1, \quad (26b)$$

$$x_i = a, z_i = \tau_i \quad i = 1, \dots, N, \quad (26c)$$

$$a, z_i, x_i, \tau_i \geq 0, \quad m_i \in \{0, 1\}, \quad i = 1, \dots, N. \quad (26d)$$

Here,  $m_i = 0$  for all  $i \in \mathcal{M}_0$  and  $m_i = 1$  for all  $i \in \mathcal{M}_1$ .  $\mathbf{z} = [z_1, \dots, z_N]'$  and  $\mathbf{x} = [x_1, \dots, x_N]'$ . With a bit abuse of notation, we denote  $\boldsymbol{\tau} = [\tau_1, \dots, \tau_N]'$ . Notice that variables  $z_i$  and  $\tau_i$  are immaterial to the objective if  $m_i = 0$ . Then, (P3) can be equivalently written as

$$\underset{a, \mathbf{z}, \mathbf{x}, \boldsymbol{\tau}, \mathbf{m}}{\text{maximize}} \quad \sum_{i=1}^N q_i(x_i, \tau_i, m_i) + g(\mathbf{z}, a) \quad (27a)$$

$$\text{subject to} \quad x_i = a, \tau_i = z_i \quad i = 1, \dots, N, \quad (27b)$$

$$x_i, \tau_i \geq 0, \quad m_i \in \{0, 1\}, \quad i = 1, \dots, N, \quad (27c)$$

where

$$q_i(x_i, \tau_i, m_i) = w_i \left\{ (1 - m_i) \eta_1 \left( \frac{h_i}{k_i} \right)^{\frac{1}{3}} x_i^{\frac{1}{3}} + m_i \varepsilon \tau_i \ln \left( 1 + \frac{\eta_2 h_i^2 x_i}{\tau_i} \right) \right\}, \quad (28)$$

and

$$g(\mathbf{z}, a) = \begin{cases} 0, & \text{if } (\mathbf{z}, a) \in \mathcal{G}, \\ -\infty, & \text{otherwise,} \end{cases} \quad (29)$$

where  $\mathcal{G} = \left\{ (\mathbf{z}, a) \mid \sum_{i=1}^N z_i + a \leq 1, a \geq 0, z_i \geq 0, i = 1, \dots, N \right\}$ .

Problem (27) can be effectively decomposed using the ADMM technique [22], which solves for the optimal solution of the dual problem. By introducing multipliers to the constraints in (27b), we can write a partial augmented Lagrangian of (27) as

$$L(\mathbf{u}, \mathbf{v}, \boldsymbol{\theta}) = \sum_{i=1}^N q_i(\mathbf{u}) + g(\mathbf{v}) + \sum_{i=1}^N \beta_i (x_i - a) + \sum_{i=1}^N \gamma_i (\tau_i - z_i) - \frac{c}{2} \sum_{i=1}^N (x_i - a)^2 - \frac{c}{2} \sum_{i=1}^N (\tau_i - z_i)^2, \quad (30)$$

where  $\mathbf{u} = \{\mathbf{x}, \boldsymbol{\tau}, \mathbf{m}\}$ ,  $\mathbf{v} = \{z, a\}$ , and  $\boldsymbol{\theta} = \{\boldsymbol{\beta}, \boldsymbol{\gamma}\}$ .  $c > 0$  is a fixed step size. The corresponding dual function is

$$d(\boldsymbol{\theta}) = \underset{\mathbf{u}, \mathbf{v}}{\text{maximize}} \left\{ L(\mathbf{u}, \mathbf{v}, \boldsymbol{\theta}) \mid \mathbf{x} \geq \mathbf{0}, \boldsymbol{\tau} \geq \mathbf{0}, \mathbf{m} \in \mathbb{B}^{N \times 1} \right\}, \quad (31)$$

where  $\mathbb{B}^{N \times 1}$  denotes a  $(N \times 1)$  binary vector. Furthermore, the dual problem is

$$\underset{\boldsymbol{\theta}}{\text{minimize}} d(\boldsymbol{\theta}). \quad (32)$$

The ADMM technique solves the dual problem (32) by iteratively updating  $\mathbf{u}$ ,  $\mathbf{v}$ , and  $\boldsymbol{\theta}$ . We denote the values in the  $l$ -th iteration as  $\{\mathbf{u}^l, \mathbf{v}^l, \boldsymbol{\theta}^l\}$ . Then, in the  $(l+1)$ -th iteration, the update of the variables is performed sequentially as follows:

1) *Step 1:* Given  $\{\mathbf{v}^l, \boldsymbol{\theta}^l\}$ , we first maximize  $L$  with respect to  $\mathbf{u}$ , where

$$\mathbf{u}^{l+1} = \arg \underset{\mathbf{u}}{\text{maximize}} L(\mathbf{u}, \mathbf{v}^l, \boldsymbol{\theta}^l). \quad (33)$$

Notice that (33) can be decomposed into  $N$  parallel subproblems. Each subproblem solves

$$\{x_i^{l+1}, \tau_i^{l+1}, m_i^{l+1}\} = \arg \underset{x_i, \tau_i \geq 0, m_i \in \{0,1\}}{\text{maximize}} s^l(x_i, \tau_i, m_i), \quad (34)$$

where

$$s_i^l(x_i, \tau_i, m_i) = q_i(x_i, \tau_i, m_i) + \beta_i^l x_i + \gamma_i^l \tau_i - \frac{c}{2} (x_i - a^l)^2 - \frac{c}{2} (\tau_i - z_i^l)^2. \quad (35)$$

By considering  $m_i = 0$  and 1, respectively, we can express (34) as

$$\begin{cases} \underset{x_i, \tau_i \geq 0}{\text{maximize}} w_i \eta_1 \left( \frac{h_i}{k_i} \right)^{\frac{1}{3}} x_i^{\frac{1}{3}} + \beta_i^l x_i + \gamma_i^l \tau_i - \frac{c}{2} (x_i - a^l)^2 - \frac{c}{2} (\tau_i - z_i^l)^2, & m_i = 0, \\ \underset{x_i, \tau_i \geq 0}{\text{maximize}} w_i \varepsilon \tau_i \ln \left( 1 + \frac{\eta_2 h_i^2 x_i}{\tau_i} \right) + \beta_i^l x_i + \gamma_i^l \tau_i - \frac{c}{2} (x_i - a^l)^2 - \frac{c}{2} (\tau_i - z_i^l)^2, & m_i = 1. \end{cases} \quad (36)$$

For both  $m_i = 0$  and 1, (36) solves a strictly convex problem, and thus the optimal solution can be easily obtained, e.g., using the projected Newton's method [21]. Accordingly, we can simply select  $m_i = 0$  or 1 that yields a larger objective value in (36) as  $m_i^{l+1}$ , and the corresponding optimal solution as  $x_i^{l+1}$  and  $\tau_i^{l+1}$ . After solving the  $N$  parallel subproblems,

the optimal solution to (33) is given by  $\mathbf{u}^{l+1} = \{\mathbf{x}^{l+1}, \boldsymbol{\tau}^{l+1}, \mathbf{m}^{l+1}\}$ . Notice that the complexity of solving each subproblem does not scale with  $N$  (i.e.,  $O(1)$  complexity), thus the overall computational complexity of Step 1 is  $O(N)$ .

2) *Step 2*: Given  $\mathbf{u}^{l+1}$ , we then maximize  $L$  with respect to  $\mathbf{v}$ . By the definition of  $g(\mathbf{v})$  in (29),  $\mathbf{v}^{l+1} \in \mathcal{G}$  must hold at the optimum. Accordingly, the maximization problem can be equivalently written as the following convex optimization problem

$$\mathbf{v}^{l+1} = \arg \underset{\mathbf{z}, a}{\text{maximize}} \quad \sum_{i=1}^N \beta_i^l (x_i^{l+1} - a) + \sum_{i=1}^N \gamma_i^l (\tau_i^{l+1} - z_i) \quad (37a)$$

$$- \frac{c}{2} \sum_{i=1}^N (x_i^{l+1} - a)^2 - \frac{c}{2} \sum_{i=1}^N (\tau_i^{l+1} - z_i)^2 \quad (37b)$$

$$\text{subject to} \quad \sum_{i=1}^N z_i + a \leq 1, \quad a \geq 0, \quad z_i \geq 0, \quad i = 1, \dots, N. \quad (37c)$$

By introducing a multiplier  $\psi$  to the constraint  $\sum_{i=1}^N z_i + a \leq 1$ , it holds at the optimum that  $a^* = \left( \frac{\sum_{i=1}^N x_i^{l+1}}{N} - \frac{\sum_{i=1}^N \beta_i^l + \psi^*}{cN} \right)^+$  and  $z_i^* = \left( \tau_i^{l+1} - \frac{\gamma_i^l + \psi^*}{c} \right)^+$ ,  $i = 1, \dots, N$ , where  $(x)^+ \triangleq \max(x, 0)$ . As  $a^*$  and  $z_i^*$  are non-increasing with  $\psi^* \geq 0$ , the optimal solution can be obtained by a bisection search over  $\psi^* > 0$  until  $\sum_{i=1}^N z_i^* + a^* = 1$  is satisfied (if possible), and then comparing the result with the case of  $\psi^* = 0$ . The details are omitted due to the page limit. Overall, the computational complexity of the method to solve (37) is  $O(N)$ .

3) *Step 3*: Finally, given  $\mathbf{u}^{l+1}$  and  $\mathbf{v}^{l+1}$ , we minimize  $L$  with respect to  $\boldsymbol{\theta}$ , which is achieved by updating the multipliers  $\boldsymbol{\theta}^l = \{\boldsymbol{\beta}^l, \boldsymbol{\gamma}^l\}$  as

$$\begin{aligned} \beta_i^{l+1} &= \beta_i^l - c(x_i^{l+1} - a^{l+1}), \quad i = 1, \dots, N, \\ \gamma_i^{l+1} &= \gamma_i^l - c(\tau_i^{l+1} - z_i^{l+1}), \quad i = 1, \dots, N. \end{aligned} \quad (38)$$

Evidently, the computational complexity of Step 3 is  $O(N)$ .

The above Steps 1 to 3 repeat until a specified stopping criterion is met. In general, the stopping criterion is specified by two thresholds: absolute tolerance (e.g.,  $\sum_{i=1}^N |x_i^l - a^l| + |\tau_i^l - z_i^l|$ ) and relative tolerance (e.g.,  $|a^l - a^{l-1}| + \sum_{i=1}^N |z_i^l - z_i^{l-1}|$ ) [22]. The pseudo-code of the ADMM method solving (P2) is illustrated in Algorithm 3. As the dual problem (32) is convex in  $\boldsymbol{\theta} = \{\boldsymbol{\beta}, \boldsymbol{\gamma}\}$ , the convergence of the proposed method is guaranteed. Meanwhile, the convergence of the ADMM method is insensitive to the choice of step size  $c$  [23]. Thus, we set  $c = \varepsilon$  without loss of generality. Besides, we can infer that the computational complexity of one ADMM iteration (including the 3 steps) is  $O(N)$ , because each of the 3 steps has  $O(N)$  complexity. Notice that

---

**Algorithm 3:** ADMM-based joint mode selection and resource allocation algorithm
 

---

**input** : The number of WDs  $N$  and other system parameters, e.g,  $h_i$ 's and  $w_i$ 's.

- 1 **initialization:**  $\{\beta^0, \gamma^0\} \leftarrow -100$ ;  $a^0 \leftarrow 0.9$ ;  $z_i^0 = (1 - a^0)/N$ ,  $i = 1, \dots, N$ ;
- 2  $c \leftarrow \varepsilon$ ,  $\sigma_1 \leftarrow 0.0005N$ ,  $l \leftarrow 0$ ;
- 3 **repeat**
- 4     **for each**  $WD_i$  **do**
- 5         Update local variables  $\{x_i^{l+1}, \tau_i^{l+1}, m_i^{l+1}\}$  by solving (36);
- 6     **end**
- 7     Update coupling variables  $\{\mathbf{z}^{l+1}, a^{l+1}\}$  by solving (37);
- 8     Update multipliers  $\{\beta^{l+1}, \gamma^{l+1}\}$  using (38);
- 9      $k \leftarrow k + 1$ ;
- 10 **until**  $\sum_{i=1}^N (|x_i^l - a^l| + |\tau_i^l - z^l|) < 2\sigma_1$  and  $|a^l - a^{l-1}| + \sum_{i=1}^N |z_i^l - z_i^{l-1}| < \sigma_1$ ;
- 11 **Return**  $\{a^l, \tau^l, \mathbf{m}^l\}$  as an approximate solution to (P3);

---

the ADMM algorithm may not exactly converge to the primal optimal solution of (P3) due to the potential duality gap of non-convex problems. Therefore, upon termination of the algorithm, the dual optimal solution  $\{a^l, \tau^l, \mathbf{m}^l\}$  is an approximate solution to (P3), whose performance gap will be evaluated through simulations.

## VI. SIMULATION RESULTS

In this section, we present simulations to verify our analysis and evaluate the performance of the proposed algorithms. In all simulations, we use the Powercast TX91501-3W transmitter with  $P = 3\text{W}$  (Watt) as the energy transmitter at the AP, and P2110 Powerharvester as the energy receiver at each WD with  $\mu = 0.51$  energy harvesting efficiency.<sup>5</sup> Without loss of generality, we set  $T = 1$ . The wireless channel gain  $h_i$  follows the free-space path loss model

$$h_i = A_d \left( \frac{3 \cdot 10^8}{4\pi f_c d_i} \right)^{d_e}, \quad i = 1, \dots, N, \quad (39)$$

where  $A_d = 4.11$  denotes the antenna gain,  $f_c = 915$  MHz denotes the carrier frequency,  $d_i$  in meters denotes the distance between the  $WD_i$  and AP, and  $d_e \geq 2$  denotes the path loss exponent. Unless otherwise stated,  $d_e = 2.8$ . Likewise, we set equal computing efficiency parameter  $k_i = 10^{-26}$ ,  $i = 1, \dots, N$ , and  $\phi = 100$  for all the WDs [15]. For the data offloading mode, the bandwidth  $B = 2$  MHz and  $v_u = 1.1$ .

<sup>5</sup>Please see the detailed product specifications on the website of Powercast Co. (<http://www.powercastco.com>).

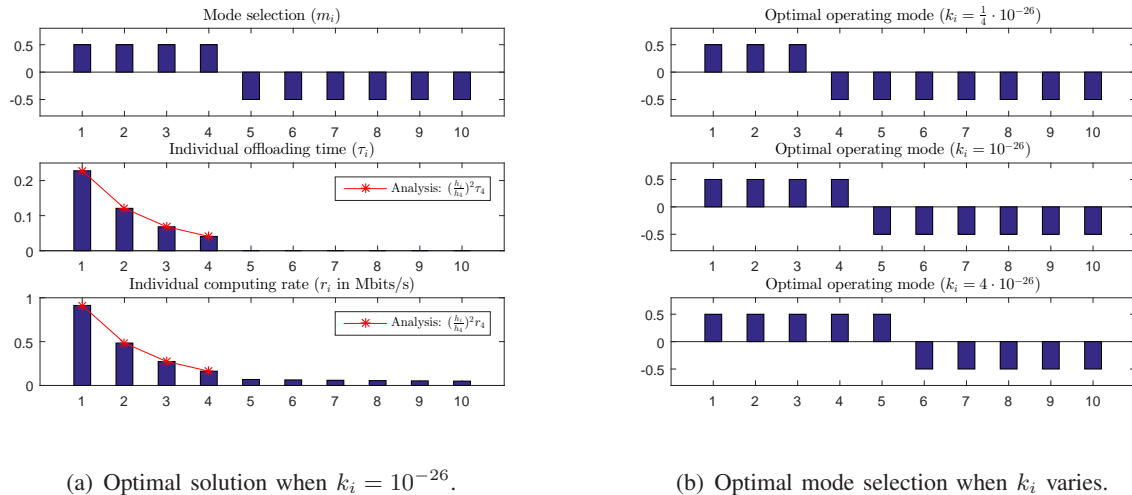


Fig. 3: Optimal solutions of the homogeneous special case of 10 WDs with equal  $k_i$  and  $w_i$ . The x-axis denotes the indices of WDs, where from WD<sub>1</sub> to WD<sub>10</sub> the wireless channel becomes weaker. The left figure shows the optimal computing mode solution (0.5 for mode 1 and  $-0.5$  for mode 0), the individual offloading time and computation rates when  $k_i = 10^{-26}$ . The right figure compares the optimal mode selection when  $k_i$  varies.

#### A. Properties of Optimal Solution

We first study some interesting properties of the optimal solution to (P2), which is obtained by enumerating all the  $2^N$  combinations of the  $N$  WDs' computing mode selections. For the simplicity of illustration, we consider  $N = 10$  and set  $d_i = 2.5 + 0.3(i - 1)$  meters,  $i = 1 \dots, 10$ . In this case, the WDs are equally spaced by 0.3 meter, where WD<sub>1</sub> ( $d_1 = 2.5$ ) has the strongest wireless channel and WD<sub>10</sub> ( $d_{10} = 5.2$ ) has the weakest wireless channel.

In Fig. 3, we first study a homogeneous special case with  $w_i = 1$  for all the WDs. In particular, we plot in Fig. 3(a) the optimal mode selection (the figure above), the offloading time (the figure in the middle), and the individual computation rate (the bottom figure) of the 10 WDs when computing efficiency  $k_i = 10^{-26}$ . In all the three sub-figures, the x-axis denotes the indices of the 10 WDs. Without loss of generality, we use  $m_i = 0.5$  and  $m_i = -0.5$  to denote that a WD <sub>$i$</sub>  selects mode 1 and 0, respectively. We can see that the optimal mode selection has a threshold structure as proved in Proposition 2, where the 4 mode-1 WDs have stronger wireless channels than the other mode-0 WDs. Besides, both the optimal offloading time and the computation rates are proportional to  $h_i^2$  for the mode-1 WDs, which matches with our analysis in Section IV.C. We also observe from the bottom figure of Fig. 3(a) that the use of edge computing significantly improves the computation rate of the mode-1 WDs. For instance, the computation rate of the mode-0 WD<sub>5</sub> is merely 7.5% higher than another mode-0 WD<sub>6</sub> because of the 0.3-meter shorter

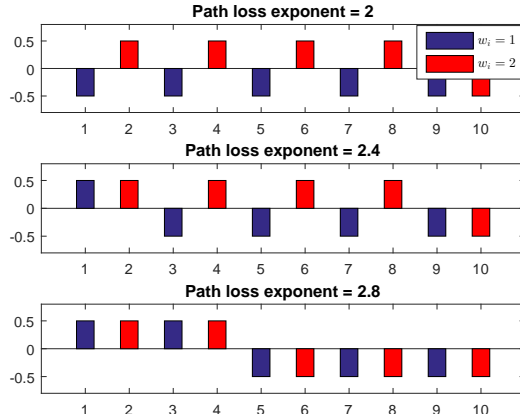
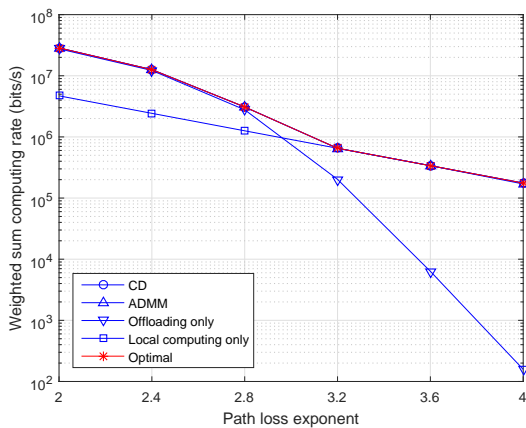


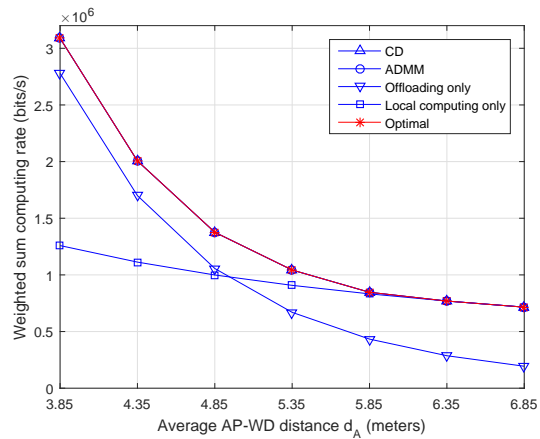
Fig. 4: Change of optimal computing modes of a heterogeneous case, where  $w_i = 1$  if  $i$  is an odd number and  $w_i = 2$  otherwise. The three figures show the performance under path loss exponent  $d_e = \{2, 2.4, 2.8\}$ , respectively.

distance to the AP. However, the computation rate of the mode-1 WD<sub>4</sub> is 135% higher than WD<sub>5</sub> despite that WD<sub>4</sub> is also 0.3-meter closer to the AP. In Fig. 3(b), we further study the impact of computing efficiency  $k_i$  to the optimal mode selection. From the top to the bottom figures,  $k_i$  increases by 16 times from  $k_i = \frac{1}{4} \cdot 10^{-26}$  to  $4 \cdot 10^{-26}$ . That is, the energy efficiency of local computing decreases. It can be seen that fewer WDs choose a local computing mode as  $k_i$  increases because of the more energy-consuming local computations. In all cases, the optimal computing mode selection remains a threshold structure, which matches our analysis in Proposition 2.

In Fig. 4, we consider a heterogeneous case, where the WDs have different weight  $w_i$ 's. For simplicity of illustration, we set  $w_i = 1$  if  $i$  is an odd number and  $w_i = 2$  otherwise. We plot the variation of optimal computing modes when the path loss exponent  $d_e \in \{2, 2.4, 2.8\}$ . Notice that a larger  $d_e$  indicates a larger channel disparity among the WDs and vice versa. We see that when the wireless channel disparity is relatively small, the weighting factor plays an important rule in the mode selection. The four WDs with higher weights operate in mode 1 when  $d_e = 2$ . However, as the channel disparity increases, wireless channel condition becomes a more dominant factor. Now the four WDs with the strongest channels operate in mode 1 when  $d_e = 2.8$ . Interestingly, the optimal mode selection also has a *threshold structure* within each group of WDs of the equal weight. For instance, when  $d_e = 2.4$ , for WDs with  $w_i = 1$ , only the WD with the strongest channel selects mode 1; while for WDs with  $w_i = 2$ , the 4 WDs with strongest channels select mode 1.



(a) Under different path loss exponent.



(b) Under different average AP-WD distance.

Fig. 5: Comparisons of computation rate performance of different algorithms. Left figure: when  $d_e$  varies. Right figure: when the average AP-to-WD distance varies, the path-loss exponent is fixed as  $d_e = 2.8$ .

### B. Computation Rate Performance Comparison

In this subsection, we evaluate the computation rate performance of the proposed algorithms. For the coordinate descent (CD) method, the initial mode selection is randomly selected, while the initial condition of ADMM-based method is specified in Algorithm 3. Besides, we consider the following three representative benchmark methods:

- 1) Optimal: exhaustively enumerates all the  $2^N$  combinations of  $N$  WDs' computing modes and outputs the best performing one;
- 2) Offloading only: all the WDs offload their tasks to the AP,  $\mathcal{M}_0 = \emptyset$ ;
- 3) Local computing only: all the WDs perform computations locally,  $\mathcal{M}_0 = \mathcal{M}$ .

In Fig. 5(a), we compare the weighted sum computation rate achieved by different schemes when the path loss exponent  $d_e$  increases from 2 to 4. Except for the varying path loss exponent  $d_e$ , the other network setups, e.g., the number of WDs, WD locations and weights, are the same as those used in Fig. 4. We see that when  $d_e$  is small and the wireless channels are strong, e.g.,  $d_e \leq 2.4$ , the offloading-only scheme achieves near optimal solution. However, as we increase  $d_e$ , the performance of the offloading-only scheme quickly degrades, e.g., achieving only around 1/1000 of the optimal rate when  $d_e = 4$ , because the offloading rates severely suffer from the weak channels in both the uplink and downlink. In contrast, the local-computing-only scheme achieves the worst performance when  $d_e$  is small (only around 1/6 of the maximum when  $d_e \leq 2.4$ ) but near-optimal performance when  $d_e \geq 3.2$ . On the other hand, the proposed CD

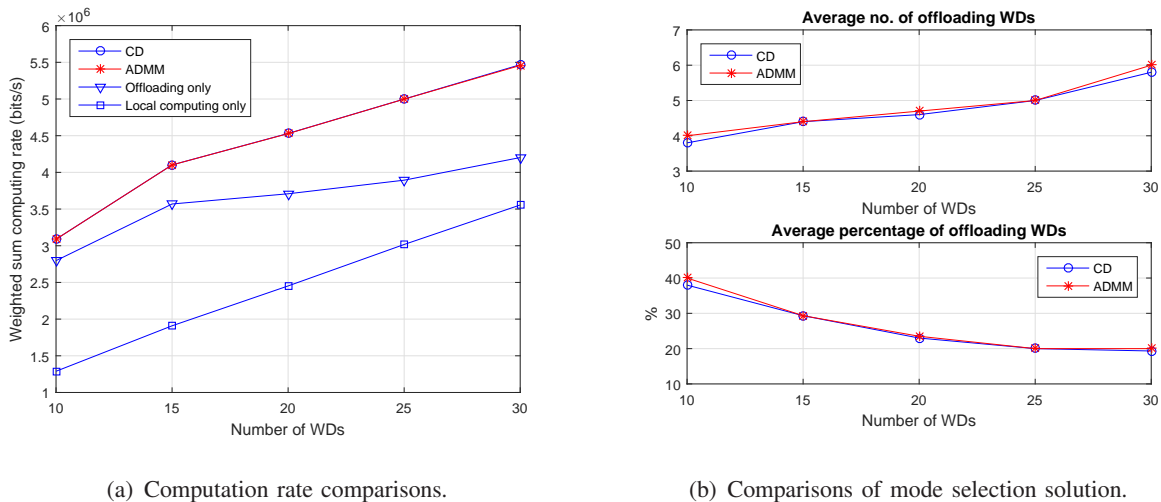


Fig. 6: Performance comparisons of different algorithms when the number of WDs varies. Left figure compares the computation rate performance. Right figure shows the average number and ratio of mode-1 WDs for CD and ADMM-based methods.

and ADMM methods both achieve near-optimal performance for all values of  $d_e$  (at most 0.5% performance gap compared to the optimal value), where the two curves are on top of each other with the optimal scheme.

In Fig. 5(b), we fix  $d_e = 2.8$  and compare the computation rate performance when the average distance  $d_A$  between the AP and the WDs varies. For simplicity of illustration, we consider 10 WDs uniformly placed within the range  $[d_A - 1.35, d_A + 1.35]$  with a 0.3 meter spacing between every two adjacent WDs. In this sense, the placement of the WDs in Fig. 3, 4 and 5(a) corresponds to the case with  $d_A = 3.85$ . The weight assignment follows that in Fig. 4 and 5(a). We observe that both the proposed CD and ADMM methods achieve near-optimal performance for all values of  $d_A$ . The offloading-only scheme achieves relatively good performance when  $d_A$  is small, e.g.,  $d_A \leq 4.35$ , but poor performance when  $d_A$  is large ( $\approx \frac{1}{3}$  of the optimal value when  $d_A = 6.85$ ). The local-computing-only scheme, however, performs poorly when  $d_A$  is small ( $\approx \frac{1}{3}$  of the optimal value when  $d_A = 3.85$ ) but achieving near-optimal solution when  $d_A$  is large. The results in Fig. 5(b) show that it is more preferable for a WD to offload computation when its wireless channel is strong and to perform local computing otherwise.

In Fig. 6, we compare the performance of different algorithms when the number of WDs  $N$  varies from 10 to 30. For each WD<sub>*i*</sub>, its distance to the AP is uniformly generated as  $d_i \sim U(2.5, 5.2)$ , and its weight  $w_i$  is randomly assigned as either 1 or 2 with equal probability. Besides, each point in the figure is an average performance of 20 independent random placements.

Specifically, we first compare the computation rate performance in Fig. 6(a). Unlike in Fig. 5, the optimal performance is not plotted because the mode-enumeration based optimal method is computationally infeasible for most values of  $N$  within the considered range. For example,  $N = 15$  requires over 30000 repeated calculations of Algorithm 1 for each WD placement. Instead, we only compare the performance of the other four sub-optimal methods. We see that the sum rates increase with the number of WDs for all the schemes considered. In particular, the proposed CD and ADMM schemes have similar performance and significantly outperform the other two benchmark methods, i.e., around 21% and 92% higher average computation rate than the offloading-only and local-computing-only schemes, respectively. In particular, the offloading-only scheme performs relatively well when  $N \leq 15$ , but the rate increase becomes slower than the other three methods when  $N$  becomes larger. To explain this observation, we plot in Fig. 6(b) the average number and ratio of mode-1 WDs under different  $N$  achieved by the ADMM and CD methods. Interestingly, for both algorithms, the number of mode-1 WDs increases almost linearly with  $N$ , i.e., approximately 1 in every 10 newly added WDs will perform task offloading. The ratio of the mode-1 WDs, however, decreases with  $N$  and gradually converges. This indicates that in a large-scale network, only a small portion of WDs perform computation offloading at the optimal operating point due to the limited system air time for task offloading. This also explains the slow increase of computation rate of offloading-only scheme when  $N$  is large.

To sum up from Fig. 5 and 6, the performance of the offloading-only and local-computing-only methods are very sensitive to the network parameters and placement, e.g., path loss exponent, distance, and network size, which may produce very poor performance in some practical setups. In contrast, using either random or fixed initial point, the proposed CD and ADMM methods can both achieve near-optimal computation rate performance under different network setups. We can infer that the computation rate performance of the two proposed methods is insensitive to the choice of initial condition. Besides, it is in general more preferable for a WD to offload computation when its wireless channel is strong and to perform local computing otherwise.

### C. Computational Complexity Evaluation

In Fig. 7, we characterize the computational complexity of the proposed CD- and ADMM-based algorithms. Here, we use the same network setup as in Fig. 6 and examine the convergence rates of the two methods when  $N$  increases. With the termination criterions in Algorithm 2 and 3, we plot the average number of computing mode swaps searched by the CD method (the number

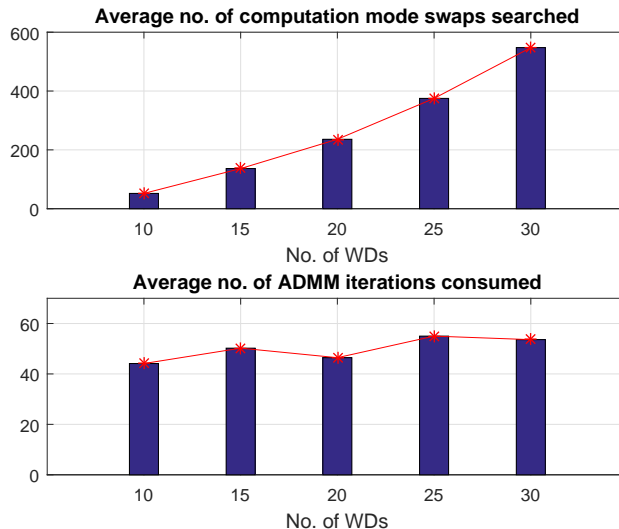


Fig. 7: Average number of iterations before convergence of the proposed CD (figure above) and ADMM (figure below) based methods when the number of WDs varies.

of calculations of Algorithm 1) and the average number of ADMM iterations consumed by the ADMM-based method before their convergence. Specifically, the iteration number of CD method is approximately a quadratic function, i.e.,  $O(N^2)$ . On the other hand, the ADMM-based method consumes almost constant number of iterations under different  $N$  within the considered range, i.e.,  $O(1)$ . As the computational complexities of both Algorithm 1 and one ADMM iteration are  $O(N)$ , the overall computational complexities of the CD- and ADMM-based methods are  $O(N^3)$  and  $O(N)$ , respectively. The results indicates that the CD method may suffer from a quick increase of computational complexity with the network size. In comparison, the computational complexity of the proposed ADMM based method increases slowly as the network size increase. Therefore, it is more preferable to apply the ADMM-based method in a large-size IoT network where the network size dominates the overall complexity.

## VII. CONCLUSIONS AND FUTURE WORK

In this paper, we studied a weighted sum computation rate maximization problem in multi-user wireless powered edge computing networks with binary computation offloading policy. We formulated the problem as a joint optimization of individual computing mode selection and system transmission time allocation. In particular, we proposed two efficient solution algorithms to tackle the difficult combinatorial computing mode selection, where one coordinate descent

method decouples the optimizations of mode selection and time allocation, and the other ADMM-based method optimizes them jointly. For a homogeneous special case, we showed that a simple linear search method achieves the globally optimal solution. Extensive simulation results showed that both the proposed CD-based and ADMM-based methods can achieve near-optimal computation rate performance under different network setups, and significantly outperform the other representative benchmark methods.

In practical implementation, the CD method requires only basic function evaluations, while the ADMM-based method needs to run more complex convex optimization algorithms. However, the ADMM-based method has a  $O(N)$  computational complexity in network size  $N$  compared to the  $O(N^3)$  complexity of the CD method. Therefore, it is more preferable to use the CD method when network size is small or the MEC server is hardware-constrained, and to use ADMM-based method in large-scale networks where the network size dominates the overall complexity.

Finally, we conclude the paper with some interesting future working directions of wireless powered MEC. First, we assumed in this paper that the MEC server has unlimited computing capacity. In practice, massive offloading tasks may overwhelm the MEC server such that it needs to allocate its computing power among the offloading tasks received. As a result, the computation delay at the MEC server becomes non-negligible, thus should be jointly considered with task offloading time. Second, it is interesting to extend the problem to fading channels, such that a WD may choose to store the harvested energy in the battery in some time slots instead of performing immediate local computing or offloading. At last, it is also challenging to extend the considered network model to other practical setups, such as multi-antenna AP, relay channel, user cooperation, and interference channel, etc.

## APPENDIX A

### PROOF OF LEMMA 1

*Proof:* The partial derivative of  $L$  with respect to  $\tau_j$  is

$$\frac{\partial L}{\partial \tau_j} = w_j \varepsilon \ln \left( 1 + \frac{\eta_2 h_j^2 a}{\tau_j} \right) - \frac{w_j \varepsilon \cdot \eta_2 h_j^2 a \tau_j^{-1}}{1 + \eta_2 h_j^2 a \tau_j^{-1}} - \nu. \quad (40)$$

By setting  $\frac{\partial L}{\partial \tau_j} = 0$  at the maximum point, we have

$$\ln \left( 1 + \eta_2 h_j^2 a \tau_j^{-1} \right) = \left( 1 + \frac{\nu}{w_j \varepsilon} \right) - \frac{1}{1 + \eta_2 h_j^2 a \tau_j^{-1}}. \quad (41)$$

By taking a natural exponential operation at both sides, we have

$$\left( 1 + \eta_2 h_j^2 a \tau_j^{-1} \right) \exp \left( \frac{1}{1 + \eta_2 h_j^2 a \tau_j^{-1}} \right) = \exp \left( 1 + \frac{\nu}{w_j \varepsilon} \right). \quad (42)$$

Consider two positive values  $x$  and  $z$  that satisfy  $\frac{1}{x} \exp(x) = z$ , it holds that

$$-x \exp(-x) = -\frac{1}{z}. \quad (43)$$

Therefore, we have  $x = -W(-\frac{1}{z})$ , where  $W(v)$  denotes the Lambert-W function, which is the inverse function of  $f(u) = u \exp(u) = v$ , i.e.,  $u = W(v)$ . Comparing (42) and (43), it is straightforward to infer that  $\frac{1}{1+\eta_2 h_j^2 a \tau_j^{-1}} = -W\left(-\frac{1}{\exp(1+\frac{\nu}{w_j \varepsilon})}\right)$ , which leads to the result in Lemma 1 with some simple manipulation. ■

## APPENDIX B

### PROOF OF PROPOSITION 2

*Proof:* It is straightforward to show that Proposition 2 holds for the two trivial cases with  $\mathcal{M}_0^* = \emptyset$  and  $\mathcal{M}_1^* = \emptyset$ . Therefore, to prove Proposition 2, it suffices to show that  $h_i \leq h_j$  holds for any  $i \in \mathcal{M}_0^*$  and  $j \in \mathcal{M}_1^*$ , where  $\mathcal{M}_0^* \neq \emptyset$  and  $\mathcal{M}_1^* \neq \emptyset$ . We denote the optimal WPT time as  $a^*T$  and the optimal offload time as  $\tau_j^*T$  for  $\text{WD}_j$ . Suppose that we swap the operating modes of  $\text{WD}_i$  and  $\text{WD}_j$ , while allowing  $\text{WD}_i$  to offload for the same amount of time  $\tau_j^*T$ . Only the two WDs' computation rates are affected by the mode swapping. Because the mode swapping provides a feasible solution to (P2), it must hold that

$$\eta_1 \left(\frac{h_i}{k}\right)^{\frac{1}{3}} (a^*)^{\frac{1}{3}} + \varepsilon \tau_j^* \ln \left(1 + \frac{\eta_2 h_j^2 a^*}{\tau_j^*}\right) \geq \eta_1 \left(\frac{h_j}{k}\right)^{\frac{1}{3}} (a^*)^{\frac{1}{3}} + \varepsilon \tau_j^* \ln \left(1 + \frac{\eta_2 h_i^2 a^*}{\tau_j^*}\right), \quad (44)$$

where the LHS and RHS of (44) correspond to the sum computation rate of  $\text{WD}_i$  and  $\text{WD}_j$  before and after the above mode swapping, respectively. We define a function

$$T(h) = h^{\frac{1}{3}} - c_1 \ln(1 + c_2 h^2), \quad h \in (0, 1), \quad (45)$$

where  $c_1 = \frac{\varepsilon \tau_j^*}{\eta_1} \left(\frac{k}{a^*}\right)^{\frac{1}{3}}$  and  $c_2 = \frac{\eta_2 a^*}{\tau_j^*} \approx 10^{10}$ . Accordingly, (44) corresponds to  $T(h_i) \geq T(h_j)$ . Notice that  $T(h_j) < 0$  must hold because otherwise we can improve the objective of (P2) by changing the computing mode of  $\text{WD}_j$  from 1 to 0. Besides, it holds that  $T(0) = 0$ .

The first order derivative  $T'(h)$  is

$$T'(h) = \frac{1}{3} h^{-\frac{2}{3}} \left(1 - \frac{6c_1 c_2 h^{\frac{5}{3}}}{1 + c_2 h^2}\right). \quad (46)$$

We define  $x = h^2$ , such that  $T'(h) > 0$  if and only if  $6c_1 x^{\frac{5}{6}} < \frac{1}{c_2} + x$ , where  $\frac{1}{c_2} \approx 10^{-10}$  is a very small value. Without loss of generality, we consider a fixed  $c_2$  and plot the only three possible cases of  $6c_1 x^{\frac{5}{6}}$  and  $\frac{1}{c_2} + x$  in Fig. 8(a) under different value of  $c_1$ , and the corresponding function value  $T(h)$  in Fig. 8(b). Notice that our considered scenario cannot be Case 1, because

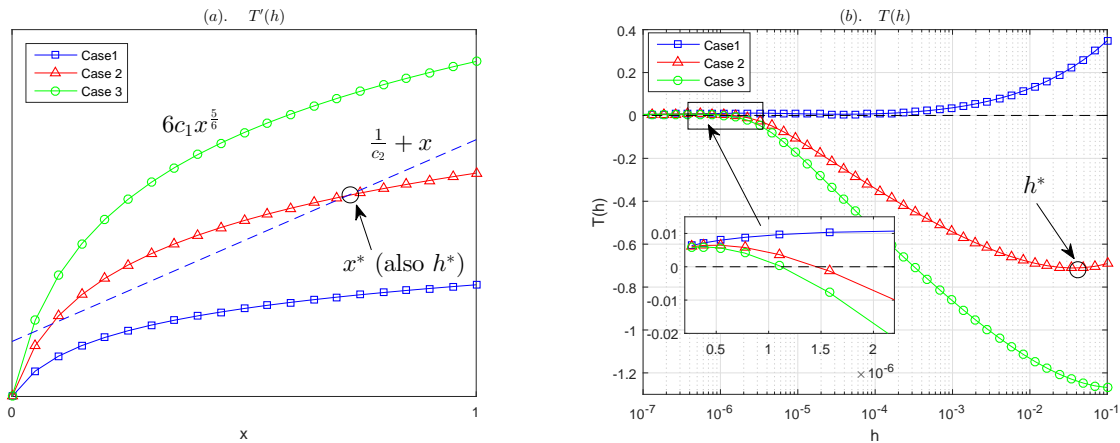


Fig. 8: Illustration of  $T(h)'$  (left) and  $T(h)$  (right) under different values of  $c_1$  in (46).

$T(h) > 0$  is a monotonically increasing function, which contracts with our knowledge that  $T(h_j) < 0$ . In Case 3,  $T(h)$  first increases to a maximum and then decreases monotonically. We can conclude from Fig. 8(b) that  $h_i \leq h_j$  given the knowledge that  $T(h_j) < 0$ . For Case 2, where  $T(h)$  first increases from  $h = 0$  to a (local) maximum, then decreases to a (local) minimum, and monotonically increases until  $h = 1$ . Here, we neglect the trivial case where  $T(h) > 0$  for all  $h \in (0, 1)$  and only consider the case that  $T(h) < 0$  holds for some  $h$  as shown in Fig. 8(b). In this case, the minimum point  $x^*$  is much larger  $\frac{1}{c_2}$ , thus we have  $6c_1(x^*)^{5/6} \approx x^*$ . Accordingly, we have the minimum of  $T(h)$  is approximately achieved at  $h^* = \sqrt{x^*} = (6c_1)^3$ . Notice that  $c_1$  cannot be too small in practical system, as otherwise local computing will always dominate computation offloading due to small offloading bandwidth (small  $\varepsilon$ ) or very efficient local computing (small  $k$ ). For a practical  $c_1 \geq 0.02$  ( $c_1 \approx 0.05$  in simulation section of this paper), the minimum of  $T(h)$  satisfies  $h^* \geq 1.7 \cdot 10^{-3}$ . Given  $T(h_i) \geq T(h_j)$  and  $T(h_j) < 0$ ,  $h_i > h_j$  if and only if  $h_i > h^*$ , such that  $10^{-3}h_i \gg 1$  holds in practice. However, this is not a realistic channel gain in a far-field wireless channel and thus ignored. Therefore,  $h_i \leq h_j$  also holds for Case 2 in a practical system, which leads to the proof of the proposition. ■

## REFERENCES

- [1] A. A. Fuqaha, M. Guizani, M. Mohammadi, M. Aledhari, and M. Ayyash, "Internet of things: a survey on enabling technologies, protocols, and applications," *IEEE Commun. Surveys Tuts.*, vol. 17, no. 4, pp. 2347-2376, 4th Quarter 2015.
- [2] S. Bi, C. K. Ho, and R. Zhang, "Wireless powered communication: opportunities and challenges," *IEEE Commun. Mag.*, vol. 53, no. 4, pp. 117-125, Apr. 2015.
- [3] X. Lu, P. Wang, D. Niyato, D. I. Kim, and Z. Han, "Wireless networks with RF energy harvesting: a contemporary survey," *IEEE Commun. Surveys Tuts.*, vol. 17, no. 2, pp. 757-789, Feb. 2015.

- [4] S. Bi, Y. Zeng, and R. Zhang, "Wireless powered communication networks:an overview," *IEEE Commun. Mag.*, vol. 23, no. 2, pp. 1536-1284, Apr. 2016.
- [5] S. Bi and R. Zhang, "Placement optimization of energy and information access points in wireless powered communication networks," *IEEE Trans. Wireless Commun.*, vol. 15, no. 3, pp. 2351-2364, Mar. 2016.
- [6] R. Zhang and C. K. Ho, "MIMO broadcasting for simultaneous wireless information and power transfer," *IEEE Trans. Wireless Commun.*, vol. 12, no. 5, pp. 1989-2001, May 2013.
- [7] Y. Zeng and R. Zhang, "Optimized training design for wireless energy transfer," *IEEE Trans. Commun.*, vol. 63, no. 2, pp. 536-550, Feb. 2015.
- [8] S. Bi and R. Zhang, "Distributed charging control in broadband wireless power transfer networks," *IEEE J. Sel. Areas in Commun.*, vol. 34, no. 12, pp. 3380-3393, Dec. 2016.
- [9] H. Ju and R. Zhang, "Throughput maximization in wireless powered communication networks," *IEEE Trans. Wireless Commun.*, vol. 13, no. 1, pp. 418-428, Jan. 2014.
- [10] L. Liu, R. Zhang, and K. Chua, "Multi-antenna wireless powered communication with energy beamforming," *IEEE Trans. Wireless Commun.*, vol. 62, no. 12, pp. 4349-4361, Dec. 2014.
- [11] M. Chiang and T. Zhang, "Fog and IoT: An overview of research opportunities," *IEEE Internet Things J.*, vol. 3, no. 6, pp. 854-864, Jun. 2016.
- [12] Y. Mao, C. You, J. Zhang, K. Huang, and K. B. Letaief, A survey on mobile edge computing: the communication perspective, submitted for publication, available on-line at [arxiv.org/abs/1701.01090](http://arxiv.org/abs/1701.01090).
- [13] ETSI white paper No. 11 (Sep. 2015). Mobile edge computing: A key technology towards 5G. available on-line at [http://www.etsi.org/images/files/ETSIWhitePapers/etsi\\_wp11\\_mec\\_a\\_key\\_technology\\_towards\\_5g.pdf](http://www.etsi.org/images/files/ETSIWhitePapers/etsi_wp11_mec_a_key_technology_towards_5g.pdf)
- [14] W. Zhang, Y. Wen, K. Guan, D. Kilper, H. Luo, and D. O. Wu, "Energy-optimal mobile cloud computing under stochastic wireless channel," *IEEE Trans. Wireless Commun.*, vol. 12, no. 9, pp. 4569-4581, Sep. 2013.
- [15] Y. Wang, M. Sheng, X. Wang, L. Wang, and J. Li, "Mobile-edge computing: partial computation offloading using dynamic voltage scaling," *IEEE Trans. Commun.*, vol. 64, no. 10, pp. 4268-4282, Oct. 2016.
- [16] C. You, K. Huang, H. Chae, and B.-H. Kim, "Energy-efficient resource allocation for mobile-edge computation offloading," *IEEE Trans. Wireless Commun.*, vol. 16, no. 3, pp. 1397-1411, Mar. 2017.
- [17] M.-H. Chen, B. Liang, and M. Dong, "Joint offloading decision and resource allocation for multi-user multi-task mobile cloud," in *Proc. IEEE Int. Conf. Commun. (ICC)*, Kuala Lumpur, Malaysia, May 2016, pp. 1-6.
- [18] C. You, K. Huang, and H. Chae, Energy efficient mobile cloud computing powered by wireless energy transfer, *IEEE J. Sel. Areas Commun.*, vol. 34, no. 5, pp. 1757-1771, May 2016.
- [19] F. Wang, J. Xu, X. Wang, and S. Cui, "Joint offloading and computing optimization in wireless powered mobile-edge computing systems," submitted for publication, available on-line at [arxiv.org/abs/1702.00606](http://arxiv.org/abs/1702.00606).
- [20] F. Wang, "Computation rate maximization for wireless powered mobile edge computing," submitted for publication, available on-line at [arxiv.org/abs/1707.05276](http://arxiv.org/abs/1707.05276).
- [21] S. Boyd and L. Vandenberghe, *Convex Optimization*, Cambridge University Press, 2004.
- [22] S. Boyd, E. Parikh, E. Chu, B. Peleato, and J. Eckstein, "Distributed optimization and statistical learning via the alternating direction method of multipliers," *Foundations and Trends in Machine Learning*, vol. 3, no. 1, pp. 1-122, Jan. 2011.
- [23] E. Ghadimi, A. Teixeira, I. Shames, and M. Johansson, "Optimal parameter selection for the alternating direction method of multipliers (ADMM): quadratic problems," *IEEE Trans. Autom. Control*, vol. 60, no. 3, pp. 644-658, Mar. 2015.